

Geometric thermodynamic uncertainty relation in periodically driven thermoelectric heat engine

Jincheng Lu,^{1,*} Zi Wang,^{1,*} Jiebin Peng,¹ Chen Wang,^{2,†} Jian-Hua Jiang,^{3,‡} and Jie Ren^{1,§}

¹*Center for Phononics and Thermal Energy Science, China-EU Joint Lab on Nanophononics, Shanghai Key Laboratory of Special Artificial Microstructure Materials and Technology, School of Physics Science and Engineering, Tongji University, Shanghai 200092, China*

²*Department of Physics, Zhejiang Normal University, Jinhua, Zhejiang 321004, China*

³*Institute of Theoretical and Applied Physics, School of Physical Science and Technology & Collaborative Innovation Center of Suzhou Nano Science and Technology, Soochow University, Suzhou 215006, China.*

(Dated: January 10, 2022)

Thermodynamic uncertainty relation, quantifying a trade-off among average current, the associated fluctuation (precision), and entropy production (cost), has been formulated in nonequilibrium steady state and various stochastic systems. Herein, we study the thermodynamic uncertainty relation in generic thermoelectric heat engines under a periodic control protocol, by uncovering the underlying Berry-phase-like contribution. We show that our thermodynamic uncertainty relation breaks the seminal steady-state results, originating from the non-vanishing geometric effect. Furthermore, by deriving the consequent trade-off relation binding efficiency, power, and constancy, we prove that the periodically driven thermoelectric heat engines can generally outperform the steady-state analogies. The general bounds are illustrated by an analytically solvable two-terminal single quantum dot heat engine under the periodic modulation. Our work provides a geometric framework in bounding and optimizing a wide range of periodically driven thermoelectric thermal machines.

I. INTRODUCTION

Periodically driven quantum machines reach limited-cycle states after a long-time evolution since the coupling to the environment prevents infinite heating up [1–5]. These limited-cycle states form the basis of various functional thermal machines, which exhibit non-negligible fluctuations [6–8]. Investigating their trade-off relations provides insights into the optimal design principles for such periodically driven systems.

Recently, a thermodynamic uncertainty relation (TUR) has been formulated based on classical Markovian steady states, which demonstrates the trade-off relation between relative current fluctuation and dissipation [9–23]. Specifically, the average current $\langle I \rangle$, its variance $\langle\langle I^2 \rangle\rangle \equiv \langle (I - \langle I \rangle)^2 \rangle$, and the entropy production rate $\langle \sigma \rangle$ is universally bounded as

$$\frac{\langle\langle I^2 \rangle\rangle}{\langle I \rangle^2} \langle \sigma \rangle \geq 2. \quad (1)$$

It is known that the TUR was initially proposed in the long-time limit [9, 24] and later generalized to the finite-time dynamics [25]. Consequently, the analysis methods

and corresponding physical implications are further refined [26–28]. Although TUR has been widely applied in tremendous amount of systems, it is not always valid. TUR violation corresponds to the situation that the left-hand side of Eq. (1) is smaller than 2. Involving quantum coherence [29], temporal driving [30–32], and magnetic field breaking time-reversal symmetry [26, 33] will violate the original TUR.

For periodically driven systems, inferring the entropy production or at least an upper bound, is generally more complex [31, 32, 34–40]. An early counterexample showed that a naive extension of the TUR from steady-state systems to periodically driven counterparts is inaccessible, since driving itself provides an spontaneous time scale enhancing current precision without significantly increasing the entropy production [41]. Subsequent attempts to find the analog for periodically driven systems yields Proesman and van den Broeck’s bound, which is valid for time-symmetric drivings [30]. Also, a series of general TUR incorporating driving speed’s effect are proposed both for discrete and continuous state spaces [31, 32, 42].

From the geometric view, the underlying the state space has an intrinsic effect on periodically driven transports and time-dependent energy conversion processes. Specifically, the geometric concepts are used in finite time thermodynamics [43, 44], in which the thermodynamic length [45] bounds the engine power and efficiency. The

* These authors contributed equally to this work.

† wangchenyifang@gmail.com

‡ jianhua.jiang@suda.edu.cn

§ xonics@tongji.edu.cn

Berry-phase-like effect provides an additional geometric contribution [46–53] to pump electric and heat currents against the thermodynamic bias. However, the intrinsic effects of geometric phase on TUR and the performance of thermal machines are largely overlooked in the previous studies. To address the geometric effect in time-dependent system, in this work, we study the thermodynamic uncertainty relation, heat-work conversion, trade-off between energy efficiency, electric work, and work fluctuations in the periodically driven thermoelectric heat engine. In particular, we find that non-vanishing geometric phase can simultaneously enhance the constancy of the engine, while not significantly introducing further entropy production.

We highlight the difference between our work and previous studies here. Firstly, our results are not restricted to time-symmetric driving protocols, in contrast to Ref. [30], which breaks down in general asymmetric protocols. Secondly, we unveil the role of geometry in driven systems, which stays unclear in previously derived TUR relations [31, 32, 42]. The geometric phase provides a versatile principle for implementing device design and optimization. Meanwhile, our framework can be readily generalized to more complex thermal machines possibly undertaking multi-tasks [54].

The paper is organized as follows. In Sec. II, we organize the TUR relationship while using the intrinsic geometric origin and analyze the bounds on electric work and energy efficiency in periodically driven thermoelectric heat engine. We study examples and verify the validity of the TUR using a two-terminal single quantum dot system in Sec. III. We conclude in Sec. IV. Throughout, we set the Boltzmann constant to 1.

II. THE UNIVERSAL BOUNDS IN PERIODICALLY DRIVEN THERMOELECTRIC HEAT ENGINE

A. The bounds on fluctuations and entropy production

For periodically driven systems with a period $\mathcal{T} \equiv 2\pi/\Omega$ [31], Koyuk and Seifert derived a family of inequalities that relate entropy production with experimentally accessible data for the mean, its dependence on driving

frequency, and the variance of a large class of observables,

$$\frac{\langle\langle I^2(\Omega) \rangle\rangle}{\langle I(\Omega) \rangle^2} \langle \sigma(\Omega) \rangle \geq 2 \left[1 - \Omega \frac{d\langle I(\Omega) \rangle}{d\Omega} \frac{1}{\langle I(\Omega) \rangle} \right]^2. \quad (2)$$

The left-hand side involves the same combination of variables as the ordinary TUR does, where the dependence on Ω is explicit. The right-hand side additionally contains the derivative of the current with respect to the driving frequency, i.e., the response of the current to a slight change of the period of driving.

The current contribution composed of two parts: the dynamic current and the geometric one, i.e., $\langle I \rangle = \langle I \rangle|_{\text{dyn}} + \langle I \rangle|_{\text{geo}}$. The dynamic part is simply an average over instantaneous steady states, whereas the geometric part originates directly from the time dependence of the cyclic state. Near the adiabatic regime, $\langle I \rangle|_{\text{dyn}}$ is independent of Ω , and the geometric current $\langle I \rangle|_{\text{geo}}$ is proportional to the driven frequency Ω [55, 56]. The reason for this scaling will be explained in later sections. Consequently, the right-hand side of Eq. (2) can be simplified as

$$1 - \Omega \frac{d\langle I(\Omega) \rangle}{d\Omega} \frac{1}{\langle I(\Omega) \rangle} = \frac{1}{1 + \langle I \rangle|_{\text{geo}}/\langle I \rangle|_{\text{dyn}}}. \quad (3)$$

Thus, we arrive at the bound

$$\frac{\langle\langle I^2 \rangle\rangle}{\langle I \rangle^2} \langle \sigma \rangle \geq 2 \left[\frac{1}{1 + \langle I \rangle|_{\text{geo}}/\langle I \rangle|_{\text{dyn}}} \right]^2 \equiv \epsilon_{\text{bound}}. \quad (4)$$

This is our first main result. In the adiabatic limit $\Omega \rightarrow 0$, we generally have $I|_{\text{geo}}/I|_{\text{dyn}} \rightarrow 0$. Therein, the geometric contribution is negligible, the dynamic part becomes dominant. Accordingly, the thermodynamic bound reproduces the ordinary TUR [9]. However, one consequence of this relation is that it provides a generic condition for (almost) dissipation-less precision. If the current is nearly proportional to the frequency of driving, where $I|_{\text{geo}} \gg I|_{\text{dyn}}$, the right-hand side vanishes. Temporally driven systems without the static bias lie in the possible implementations where this optimal limit can hold. This phenomenon is nonexistent at the steady states.

B. The bounds on electric work and energy efficiency in periodically driven thermoelectric heat engine

We consider a system isothermally coupled to several reservoirs with which it can exchange particle and energy. The total entropy production $\langle \sigma \rangle$ is specified by the stochastic thermodynamics [4]

$$T\langle \sigma \rangle = -\langle W_{\text{out}} \rangle + \langle W_d \rangle + \langle W_I \rangle. \quad (5)$$

In the right-hand side, the first term denotes the output work $\langle W_{\text{out}} \rangle$ (useful work), the second term $\langle W_d \rangle$ represents dissipation (dissipated work), and the last term is the input energy $\langle W_I \rangle$ (done by the temporal driving) accumulated over one period. T is the temperature of the reservoirs. We restrict here to cyclic states, where the average entropy production of the middle system is zero in a full cyclic period. The positive energy is defined by flowing from the reservoirs into the system.

In this subsection, we consider the heat engine regime ($\langle W_{\text{out}} \rangle > 0$). Concentrating on the work fluctuations using Eq. (2), we obtain

$$\frac{\langle \langle W_{\text{out}}^2 \rangle \rangle}{\langle W_{\text{out}} \rangle^2} \langle \sigma \rangle \geq 2 \left[1 - \Omega \frac{d\langle W_{\text{out}}(\Omega) \rangle / d\Omega}{\langle W_{\text{out}}(\Omega) \rangle} \right]^2. \quad (6)$$

(i) While the input driving energy is positive, i.e., $\langle W_I \rangle > 0$, the free energy efficiency of the heat engine is [24]

$$\langle \eta \rangle = \frac{\langle W_{\text{out}} \rangle}{\langle W_d \rangle + \langle W_I \rangle} = \frac{\langle W_{\text{out}} \rangle}{T \langle \sigma \rangle + \langle W_{\text{out}} \rangle}. \quad (7)$$

According to the above definition of efficiency $\langle \eta \rangle$, the relation Eq. (6) implies

$$\frac{1}{\langle \eta \rangle} \geq 2T \frac{\langle W_{\text{out}} \rangle}{\langle \langle W_{\text{out}}^2 \rangle \rangle} \left[1 - \Omega \frac{d\langle W_{\text{out}}(\Omega) \rangle / d\Omega}{\langle W_{\text{out}}(\Omega) \rangle} \right]^2 + 1. \quad (8)$$

Furthermore, the output work contributions come from the dynamic part and the geometric one, i.e., $W_{\text{out}} = W_{\text{out}}|_{\text{dyn}} + W_{\text{out}}|_{\text{geo}}$, and the geometric work W_{out} is proportional to the driven frequency Ω . Then, the right-hand side of Eq. (8) can be simplified as

$$\frac{1}{\langle \eta \rangle} \geq 1 + 2T \frac{\langle W_{\text{out}} \rangle}{\langle \langle W_{\text{out}}^2 \rangle \rangle} \times \left[\frac{1}{1 + \langle W_{\text{out}}(\Omega) \rangle|_{\text{geo}} / \langle W_{\text{out}}(\Omega) \rangle|_{\text{dyn}}} \right]^2 \equiv \frac{1}{\eta_{\text{bound}}}, \quad (9)$$

when $\langle W_I \rangle > 0$.

(ii) While the driving energy is negative, i.e., $\langle W_I \rangle < 0$, the free energy efficiency of the heat engine is [57, 58],

$$\langle \eta \rangle = \frac{\langle W_{\text{out}} \rangle}{\langle W_d \rangle} = \frac{\langle W_{\text{out}} \rangle}{T \langle \sigma \rangle + \langle W_{\text{out}} \rangle - \langle W_I \rangle}. \quad (10)$$

Combined with the expression of the efficiency $\langle \eta \rangle$, the relation Eq.(6) implies

$$\frac{1}{\langle \eta \rangle} \geq 2T \frac{\langle W_{\text{out}} \rangle}{\langle \langle W_{\text{out}}^2 \rangle \rangle} \left[1 - \Omega \frac{d\langle W_{\text{out}}(\Omega) \rangle / d\Omega}{\langle W_{\text{out}}(\Omega) \rangle} \right]^2 - \frac{\langle W_I \rangle}{\langle W_{\text{out}} \rangle} + 1. \quad (11)$$

By further specifying two components in the output work, the Eq. (11) can be simplified as

$$\begin{aligned} \frac{1}{\langle \eta \rangle} &\geq 1 + 2T \frac{\langle W_{\text{out}} \rangle}{\langle \langle W_{\text{out}}^2 \rangle \rangle} \\ &\times \left[\frac{1}{1 + \langle W_{\text{out}}(\Omega) \rangle|_{\text{geo}} / \langle W_{\text{out}}(\Omega) \rangle|_{\text{dyn}}} \right]^2 \\ &- \frac{\langle W_I \rangle}{\langle W_{\text{out}} \rangle|_{\text{dyn}} + \langle W_{\text{out}} \rangle|_{\text{geo}}} \equiv \frac{1}{\eta_{\text{bound}}}. \end{aligned} \quad (12)$$

Eqs. (9) and (12) are our second main results. In general, the output work of a steady-state heat engine vanishes at least linearly as its energy efficiency approaches unity [59–61]. A finite power in this limit is, in principle, is possible only if the current fluctuations diverge [13] or if the output power is proportional to the cycling frequency of the engine [31]. Although these general results have been demonstrated in previous studies, our work provides a general realizable optimization principle. By maximizing the geometric contribution $W_{\text{out}}|_{\text{geo}}$ using geometric methods and minimizing the dynamic contribution $W_{\text{out}}|_{\text{dyn}}$, we can push the bounds [Eqs. (9) and (12)] to a more efficient regime.

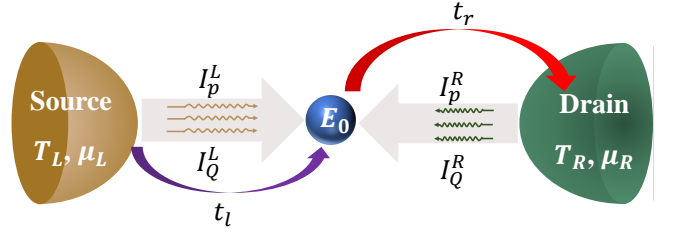


FIG. 1. Schematic of the single-level QD system. An electron from the source (with chemical potential μ_L and temperature T_L) can flow across the QD (with energy E_0) and hop into the drain (with chemical potential μ_R and temperature T_R). The energy level in the QD, E_0 , and the coupling t_i ($i = l, r$) between the dot and the reservoir, can generally be taken as time-dependent driving parameters.

III. VERIFYING THE VALIDITY OF THE THERMODYNAMIC UNCERTAINTY RELATION IN PERIODICALLY DRIVEN THERMOELECTRIC HEAT ENGINE

A. Single-level quantum dot System

We illustrate the formal results within the two-terminal system. In our construction (see Fig. 1), a single quantum dot (QD) system is exchanging energy with two electronic reservoirs, L and R , which can be set out

of equilibrium with a finite voltage bias $\Delta\mu = \mu_R - \mu_L$ or/and temperature difference $\Delta T = T_L - T_R$. Our model is described by the Hamiltonian

$$\hat{H} = \hat{H}_S + \hat{H}_B + \hat{H}_I, \quad (13)$$

where $\hat{H}_S = E_0 c_d^\dagger c_d$ denotes the sigle-level QD, $\hat{H}_B = \sum_{v=L,R} \sum_k \epsilon_{kv} c_{kv}^\dagger c_{kv}$ represents the left and right electronic reservoirs (source and drain), and $\hat{H}_I = \sum_{v=L,R} \sum_k t_{kv} (c_{kv}^\dagger c_d + \text{H.c.})$ is the system-reservoir interaction Hamiltonian. The working substance consists of a single electronic level with the annihilation operator c_d and time-dependent energy $E_0(t)$. The dot is alternating its coupling to two fermionic baths (leads) $v = L, R$, which may have different temperatures. c_{kv} annihilates an electron with energy ϵ_{kv} in the v -lead that couples to the central level with t_{kv} being the tunneling rate. The v -lead is characterized as the Fermi-Dirac distribution function $f_v(\omega) = \{\exp[(\omega - \mu_v)/k_B T_v] + 1\}^{-1}$, with an temperature T_v and a chemical potential μ_v . The reservoirs containing large number of states exert dissipative effects on the dynamics described by the spectral function $\Gamma_v(\epsilon) = 2\pi \sum_k t_{kv}^2 \delta(\epsilon - \epsilon_k)$.

Using the Redfield approximation for weak system-bath coupling [62–65], the underlying dynamics can be modeled as

$$\dot{p}_0^\lambda(t) = -k_u p_0^\lambda(t) + k_d^\lambda p_1^\lambda(t), \quad (14a)$$

$$\dot{p}_1^\lambda(t) = k_u^\lambda p_0^\lambda(t) - k_d p_1^\lambda(t). \quad (14b)$$

Here λ is the counting parameter, which can be used to calculate the fluctuation properties of an arbitrary flow, heat, particle, etc., induced by quantum transitions. These equations can be reexpressed in a matrix form as

$$\frac{d|p^\lambda(t)\rangle}{dt} = \mathcal{H}(\lambda)|p^\lambda(t)\rangle, \quad (15)$$

where $|p^\lambda(t)\rangle = (p_0^\lambda(t), p_1^\lambda(t))$. And p_n ($n = 0, 1$) denotes the probability of QD to occupy the state $|n\rangle$, satisfying $p_0(t) + p_1(t) = 1$ [66]. The activation and relaxation rates with the counting field read

$$k_u^\lambda = k_{0 \rightarrow 1}^L + k_{0 \rightarrow 1}^R e^{i\lambda_p + iE_0\lambda_E}, \quad (16a)$$

$$k_d^\lambda = k_{1 \rightarrow 0}^L + k_{1 \rightarrow 0}^R e^{-i\lambda_p - iE_0\lambda_E}, \quad (16b)$$

Here, $k_{0 \rightarrow 1}^v = \Gamma_v f_v(E_0)$, and $k_{1 \rightarrow 0}^v = \Gamma_v [1 - f_v(E_0)]$ [67–70]. λ_E and λ_p are the counting fields for energy and particles, respectively. Without loss of generality, here we count the flow between the system and the right reservoir. Here we define the positive current to be flowing from reservoirs into the middle system.

Finally, the steady-state particle and energy currents flowing from the right reservoir into the system are expressed as [71, 72]

$$\langle I_p^R \rangle_s = \frac{\Gamma_L \Gamma_R [f_R(E_0) - f_L(E_0)]}{\Gamma_L + \Gamma_R}, \quad (17a)$$

$$\langle I_E^R \rangle_s = \frac{E_0 \Gamma_L \Gamma_R [f_R(E_0) - f_L(E_0)]}{\Gamma_L + \Gamma_R}, \quad (17b)$$

while $\langle I_Q \rangle$ is the net heat current carried by the electrons, $\langle I_Q^R \rangle = \langle I_E^R \rangle - \mu_R \langle I_p^R \rangle$. These steady state results are of the typical Landauer type in thermal transports [63]. The flows from the left and right reservoirs are not independent. Particle conservation implies that $\langle I_p^L \rangle_s + \langle I_p^R \rangle_s = 0$, while energy conservation requires $\langle I_E^L \rangle_s + \langle I_E^R \rangle_s = 0$ [6, 73].

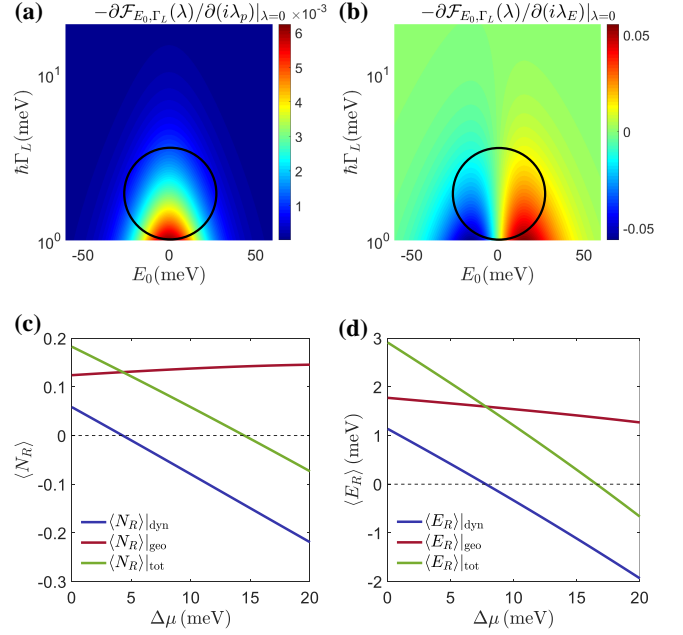


FIG. 2. The contour map of (a) Berry curvature for the average particle current: $-\partial\mathcal{F}_{E_0\Gamma_L}(\lambda)/\partial(i\lambda_p)|_{\lambda=0}$. (b) Berry curvature for the average energy current: $-\partial\mathcal{F}_{E_0\Gamma_L}(\lambda)/\partial(i\lambda_E)|_{\lambda=0}$, in the parameter space of the dot energy level E_0 and the left reservoir's spectral function Γ_L . (c) The particle current N_R . (d) The energy current E_R as a function of $\Delta\mu$. Here, we define positive flows to be from the right to the left. The parameters are $\mu = 0$ (mean value), $\hbar\Gamma_R = 1$ meV, $k_B T_L = 10$ meV and $k_B T_R = 1.5k_B T_L$. The energy modulations: $E_0 = [15 + 15 \cos(\Omega t)]$ meV, $\hbar\Gamma_L = [2 + \sin(\Omega t)]$ meV, $\Omega = 2\pi/\mathcal{T}_p$ and $\mathcal{T}_p = 10^{-12}$ s.

B. Geometric Berry-phase-induced particle and energy currents

For heat engine operation, the single QD system connected to the two reservoirs is subjected to cyclic parameter modulations. This could be realized by imposing a modulation on either of the following parameters: $\Gamma_v(t)$, $\mu_v(t)$, $T_v(t)$, ($v = L, R$) and $E_0(t)$ [74, 75]. The particle and energy currents from the right (R) reservoir into the single QD system during the long time span τ . The characteristic function is [76]

$$\mathcal{Z}_\tau = \sum_{q=-\infty}^{+\infty} P_\tau(q) e^{iq\lambda} = 1^\dagger \hat{T} [e^{\int_0^\tau \mathcal{H}(\lambda, t) dt}] \mathbf{p}(0). \quad (18)$$

where $P_\tau(q)$ is the probability distribution of having current transferred from the R reservoir into the single quantum dot system during time $\tau \rightarrow \infty$. Here $1^\dagger = [1, 1]$, \hat{T} denotes the time-ordering operator, and $\mathbf{p}(0) = [p_0(0), p_1(0)]^T$ are the initial occupation probabilities.

According to the large deviation principle and the adiabatic perturbation theory, the cumulant generating function are composed of two parts in the long time (τ) limit [49, 76],

$$\begin{aligned} \mathcal{Z}_\tau &\approx e^{\tau \mathcal{G}} = e^{\tau(\mathcal{G}_{\text{dyn}} + \mathcal{G}_{\text{geo}})}, \\ \mathcal{G}_{\text{dyn}} &= \mathcal{T}_p^{-1} \int_0^{\tau_p} dt \chi(\lambda, t), \\ \mathcal{G}_{\text{geo}} &= -\mathcal{T}_p^{-1} \int_0^{\tau_p} dt \langle \varphi(\lambda) | \partial_t | \psi(\lambda) \rangle. \end{aligned} \quad (19)$$

Here χ denotes the eigenvalues of the evolution matrix \mathcal{H} with the biggest real part. $|\psi(\lambda, t)\rangle$ and $\langle \varphi(\lambda, t)|$ are the corresponding normalized right and left eigenvector, respectively. Obviously, given a parameter path \mathcal{G}_{dyn} is independent of the driving frequency Ω , while $\mathcal{G}_{\text{geom}}$ has a factor \mathcal{T}_p^{-1} and is thus proportional to Ω . This argument solidifies the scaling properties of $\langle I \rangle|_{\text{dyn}}$ and $\langle I \rangle|_{\text{geo}}$ in our deriving TUR relations (Sec. II).

The first contribution \mathcal{G}_{dyn} presents the temporal average and defines the dynamic particle and heat transfer. This is the only term which survives in the static limit. The second, geometric part \mathcal{G}_{geo} presents an additional contribution caused by the adiabatic cyclic evolution and it requires at least two parameter modulations. For the case of periodically driving pairs $[u_1(t), u_2(t)]$, which could be chosen from quantum dot energy $[E_0(t)]$ and tunneling rate $[\Gamma_L(t)]$, we have

$$\mathcal{G}_{\text{geo}} = -\mathcal{T}_p^{-1} \iint_{u_1 u_2} du_1 du_2 \mathcal{F}_{u_1 u_2}(\lambda), \quad (20)$$

$$\mathcal{F}_{u_1 u_2} = \langle \partial_{u_1} \varphi | \partial_{u_2} \psi \rangle - \langle \partial_{u_2} \varphi | \partial_{u_1} \psi \rangle, \quad (21)$$

where $\mathcal{F}_{u_1 u_2}$ is analogous with the gauge invariant Berry curvature [77, 78]. The particle current flowing from the right reservoir into the system emerges as

$$I_p^R(t) = \frac{\partial(\mathcal{G}_{\text{dyn}} + \mathcal{G}_{\text{geo}})}{\partial(i\lambda_p)}|_{\lambda=0}, \quad (22)$$

and the energy current is

$$I_E^R(t) = \frac{\partial(\mathcal{G}_{\text{dyn}} + \mathcal{G}_{\text{geo}})}{\partial(i\lambda_E)}|_{\lambda=0}. \quad (23)$$

The electronic heat current extracted from the right reservoir is defined as $I_Q^R(t) = I_E^R(t) - \mu_R I_p^R(t)$. The particle current I_p^L and energy current I_E^L flowing from the left (L) reservoir into the central system can be achieved upon introducing the activation and relaxation rates with the counting field $k_u^\lambda = k_{0 \rightarrow 1}^L e^{i\lambda_p + iE_0\lambda_E} + k_{0 \rightarrow 1}^R$, $k_d^\lambda = k_{1 \rightarrow 0}^L e^{-i\lambda_p - iE_0\lambda_E} + k_{1 \rightarrow 0}^R$. The fluctuation of the current is $\langle \langle I^2 \rangle \rangle = \partial^2 \mathcal{G} / \partial(i\lambda)^2|_{\lambda=0}$, where $\langle \langle I^2 \rangle \rangle = \langle I^2 \rangle - \langle I \rangle^2$ is the second cumulant.

We now turn to the first law of thermodynamics for time-dependent quantum thermal machine [72]. The particle conservation is characterized as

$$\int_0^t d\tau [I_p^L(\tau) + I_p^R(\tau)] = \Delta n, \quad (24)$$

and the energy conservation is quantified by [52, 58, 79–81]

$$\int_0^t d\tau \left[\sum_{v=L,R} I_E^v(\tau) + A(\tau) \right] = \Delta U, \quad (25)$$

where Δn and ΔU are respectively the stochastic occupation number and energy change of the middle system during $[0, t]$. The input power induced by temporal driving provides an extra term $A(t)$. Since terms in the left hand sides of Eq. (24) and (25) are growing with time and the right-hand sides are naturally bounded by the size of the middle system, we arrive at the approximate conservation laws in the long time (large period number) limit [82, 83]

$$\begin{aligned} \langle N_L \rangle + \langle N_R \rangle &= 0, \\ \langle E_L \rangle + \langle E_R \rangle + \langle W_I \rangle &= 0. \end{aligned} \quad (26)$$

Here, $\langle N_v \rangle$ is the average accumulated input particle number into reservoir v , $\langle E_v \rangle$ is the input energy flowing from reservoir v and $\langle W_I \rangle$ is the extra work done by driving. These stochastic quantities are accumulated during a given time interval.

We proceed by presenting simulation results at finite temperature and bias, focusing on the large-bias limit rather than the linear-response behavior. For convenience, We define the chemical potential difference $\Delta\mu = \mu_L - \mu_R$ and the mean chemical potential $\mu \equiv (\mu_L + \mu_R)/2$. We fix the mean chemical potential μ at zero, and study the effect of $\Delta\mu$. To operate the device as a thermoelectric engine, we assume $T_L < T_R$ and $\Delta\mu > 0$. The produced electronic work after a period of driving cycle of the thermoelectric heat engine is [57, 84]

$$\langle W_{\text{out}} \rangle = -(\mu_R - \mu_L) \langle N_R \rangle. \quad (27)$$

In Fig. 2, we demonstrate the geometric thermoelectric pump effect. In Figs. 2(a) and 2(b), we illustrate that by modulating parameters of the system (the system-reservoir coupling strength Γ_L , and the QD energy level E_0), the non-trivial Berry curvature leads to both non-vanishing geometric particle and energy flow, as shown in Figs. 2(c) and 2(d). We note that the geometric flow currently can be experimentally observed [53], and our setup is within the reach of current experiment platforms [85–87].

As a main result we demonstrate that the Berry-phase effect acts as a reconfigurable pump, providing additional particle and electronic heat currents across the QD systems with no static bias or even against the direction of biases. This shows the power of our framework. By tailoring the driving path in the parameter space, we can both design the functionality of thermoelectric engines, modulate the ratio of the geometric and the dynamic components of flows, and therefore optimize the engine's performance bounds proposed in Sec. II. We elaborate this point in the following sections.

C. Verifying the validity of the TUR relationship

In Figs. 3 and 4, we verify the bounds on fluctuations and entropy production in periodically driven systems. We concentrate on the effect geometric properties, which can be characterized by the relative phases ϕ . Different ϕ represents different driving protocols. Specifically, parameters are driven as $[u_1(\Omega t), u_2(\Omega t + \phi)]$, with $u_1(\Omega t)$ and $u_2(\Omega t)$ being in phase. $\phi = \pi/2$ is the situation where the geometric contribution is optimized; in contrast, if the phase $\phi = 0$, the geometric contribution vanishes and there is *only* the dynamic one. This is obvious since the encircled area in the parameter space vanishes if $\phi = 0$.

In this work, we focus our discussions on the working regime of periodically driven thermoelectric heat engine,

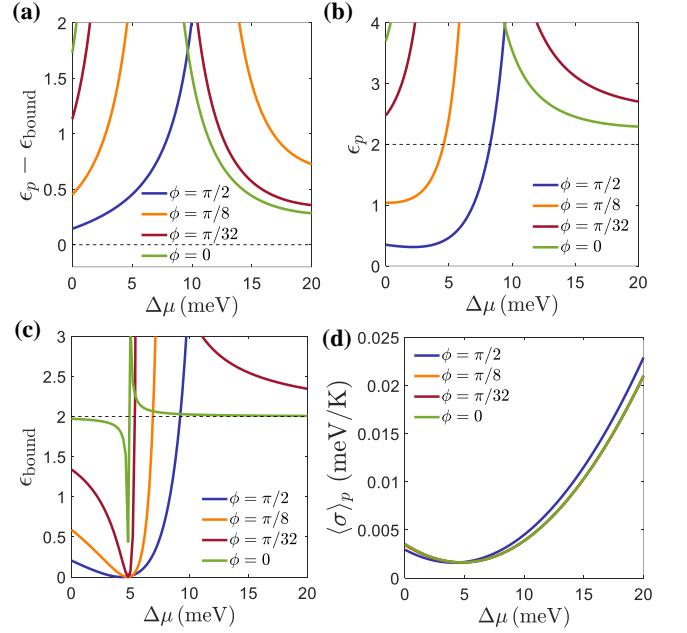


FIG. 3. (a) The distance of realized ϵ_p from the geometric TUR bound, i.e. $\epsilon_p - \epsilon_{\text{bound}}$, (b) the original TUR bound ϵ_p , (c) The bound ϵ_{bound} , (d) the average entropy production $\langle \sigma \rangle_p$ as a function of $\Delta\mu$ for different phase ϕ . The parameters are $\mu = 0$, $\hbar\Gamma_R = 1$ meV, $k_B T_L = 10$ meV and $k_B T_R = 15$ meV, $E_0 = [15 + 15 \sin(\Omega t + \phi)]$ meV, $\hbar\Gamma_L = [2 + \sin(\Omega t)]$ meV, $\Omega = 2\pi/\mathcal{T}_p$ and $\mathcal{T}_p = 10^{-12}$ s.

i.e., $\langle W_{\text{out}} \rangle > 0$. To assess our derived general bound, we denote the relative fluctuation as

$$\epsilon_p \equiv \langle \langle W_{\text{out}}^2 \rangle \rangle \langle \sigma \rangle / \langle W_{\text{out}} \rangle^2. \quad (28)$$

Here, W_{out} is the useful output work of the stochastic thermoelectric work. From Figs. 3(a) and 4(a), we find that, regardless of phase ϕ , voltage bias $\Delta\mu$, and the driving frequency Ω , the proposed geometric TUR bound $\epsilon_p - \epsilon_{\text{bound}}$, derived from Eq. (4), is always greater than zero. The bounds on fluctuations and entropy production are always satisfied. Moreover, as shown in Fig. 3(b), if the geometric current vanishes ($\phi = 0$), the steady-state TUR Eq. (1) holds. This is consistent with steady-state transport for classical Markov processes [9, 24]. Likewise, the inset figure of Fig. 4(b) illustrates that in the adiabatic limit $\Omega \rightarrow 0$, $\langle I \rangle|_{\text{geo}} / \langle I \rangle|_{\text{dyn}} \rightarrow 0$, reducing our TURs to the steady-state result. However, as the phase ϕ becomes finite, e.g., $\phi = \pi/8$ and $\phi = \pi/2$, the geometric contribution dominates the heat transport and fluctuations. Accordingly, the original TUR bound breaks down, since ϵ_p is lesser than 2 for the small voltage bias. In sharp contrast, our geometric TUR is still

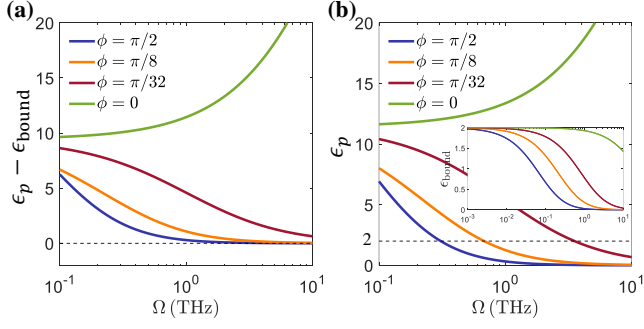


FIG. 4. (a) The distance of realized ϵ from the geometric TUR bound, i.e. $\epsilon_p - \epsilon_{\text{bound}}$, and (b) the original TUR bound ϵ_p , as a function of deriving frequency Ω for different phase ϕ . Inset: the geometric TUR bound ϵ_{bound} as a function of deriving frequency Ω . The parameters are $\Delta\mu = 3$ meV, $\mu = 0$, $\hbar\Gamma_R = 1$ meV, $k_B T_L = 10$ meV and $k_B T_R = 15$ meV, $E_0 = [15 + 15 \sin(\Omega t + \phi)]$ meV, $\hbar\Gamma_L = [2 + \sin(\Omega t)]$ meV, and $\Omega = 2\pi/\mathcal{T}_p$.

robust. Furthermore, in the regime of high driving frequency, the geometric-phase effect is pronounced, and it exactly the reason for breaking steady-state TUR [Eq. 1] and enhancing the precision of engines ($\epsilon_p < 2$).

Then, we consider harvesting the heat from the (hot) reservoir and the energy for regulating QD system to generate electricity. The entropy production of the whole system is $\langle\sigma\rangle_p = -\sum_{v=L,R} \langle Q_v \rangle / T_v$ [88]. Considering the energy and particle conversations [Eq. (26)], the entropy production is given by a specific form of Eq. (5)

$$T_L \langle\sigma\rangle_p = -\langle W_{\text{out}} \rangle + (1 - T_L/T_R) \langle Q_R \rangle + \langle W_I \rangle. \quad (29)$$

The thermal machine can be operated as a heat engine, the electric power $\langle W_{\text{out}} \rangle > 0$. If the input energy is negative, i.e., $\langle W_I \rangle < 0$, the free energy efficiency of the heat engine is specified as [84, 89–91]

$$\langle\eta\rangle_p = \frac{\langle W_{\text{out}} \rangle}{(1 - T_L/T_R) \langle Q_R \rangle}, \quad (30)$$

which is consistent with the energy efficiency of steady-state thermoelectric transport [92, 93]. While the input energy is positive, i.e., $W_I > 0$, the free energy efficiency of the heat engine is obtained as [57]

$$\langle\eta\rangle_p = \frac{\langle W_{\text{out}} \rangle}{(1 - T_L/T_R) \langle Q_R \rangle + \langle W_I \rangle}. \quad (31)$$

According to the thermodynamic second law, the thermoelectric engine efficiency is upper bounded, i.e., $\langle\eta\rangle_p \leq 1$ [72]. However, we note that the information on the geometric effect can refine this bound.

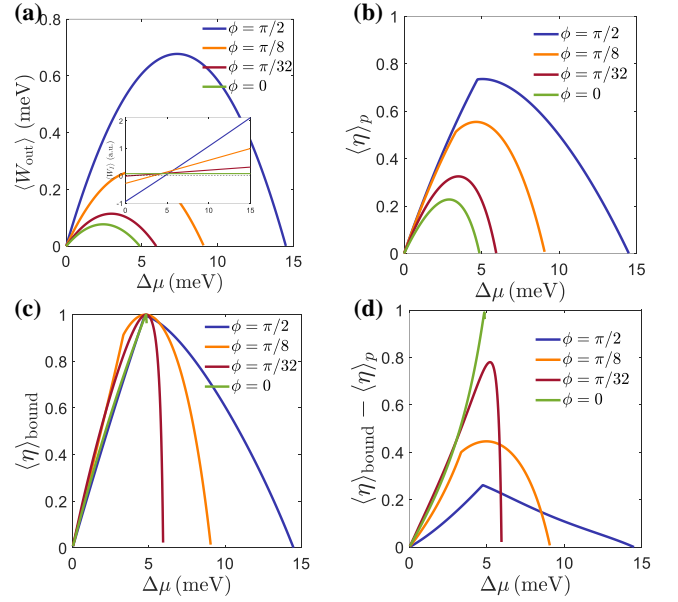


FIG. 5. (a) The output electric work $\langle W_{\text{out}} \rangle$, (b) The energy efficiency $\langle\eta\rangle_p$, (c) $\langle\eta\rangle_{\text{bound}}$, and (d) $\langle\eta\rangle_{\text{bound}} - \langle\eta\rangle_p$ as a function of $\Delta\mu$ for different ϕ . The parameters are $\mu = 0$, $\hbar\Gamma_R = 1$ meV, $k_B T_L = 10$ meV, $k_B T_R = 1.5 k_B T_L$, $E_0 = [15 + 15 \sin(\Omega t + \phi)]$ meV, $\hbar\Gamma_L = [2 + \sin(\Omega t)]$ meV, $\Omega = 2\pi/\mathcal{T}_p$ and $\mathcal{T}_p = 10^{-12}$ s.

We now illustrate the geometric bound on efficiency in Eqs. (8) and (11). As shown in Fig. 5(a) and 6(a), we respectively illustrate the effect of voltage bias $\Delta\mu$ and driving frequency Ω on the electric work $\langle W_{\text{out}} \rangle$ per driving period. Similarly, we also show $\langle\eta\rangle_p$ in Figs. 5(b) and 6(b). Obviously, the geometric phase yields significant improvement of the maximum efficiency and output work. From the efficiency change curve of Fig. 5(b), we find there is a turning point when the efficiency nearly reaches the summit. The reason for this phenomenon is that the input energy of the driving system changes from output to input, that is, the symbol of $\langle W_I \rangle$ is changed, which is illustrated in the inset of Fig. 5(a).

In Figs. 5(c-d) and Figs. 6(c-d), we plot efficiency bound η_{bound} and their difference $\eta_{\text{bound}} - \langle\eta\rangle_p$ as a function of voltage bias $\Delta\mu$ and deriving frequency Ω for a thermoelectric engine, respectively. In parameter regime of the heat engine, the energy efficiency $\langle\eta\rangle_p$ never break through the boundary η_{bound} , these simulations exemplify the validity of the geometric bounds. Interestingly, as shown in Figs. 5(d) and 6(d), the efficiency comes even closer to its bound, i.e., $\eta_{\text{bound}} - \langle\eta\rangle_p$ approaching zero, if we optimize the geometric effect via increasing either the driving frequency or ϕ .

Finally, we discuss the thermodynamic bounds of ϵ_p

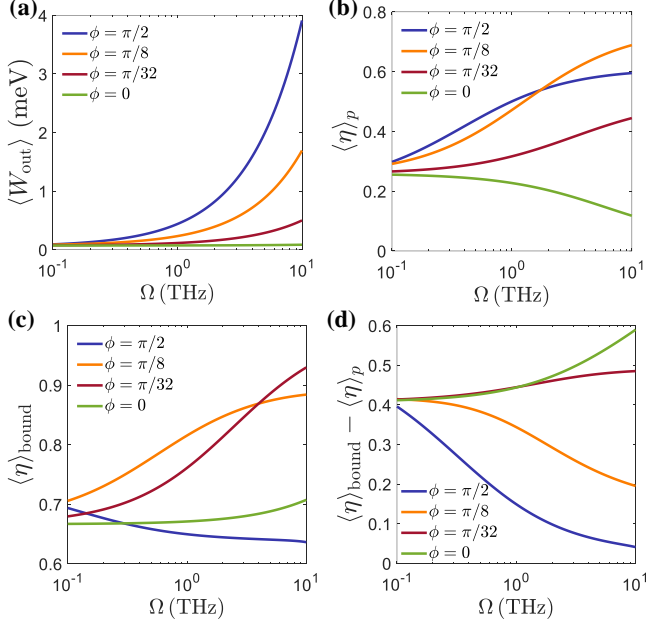


FIG. 6. (a) The output electric work $\langle W_{\text{out}} \rangle$, (b) the energy efficiency $\langle \eta \rangle_p$, (c) $\langle \eta \rangle_{\text{bound}}$, and (d) $\langle \eta \rangle_{\text{bound}} - \langle \eta \rangle_p$ as a function of driving frequency Ω for different phase ϕ . The parameters are $\Delta\mu = 3$ meV, $\mu = 0$, $\hbar\Gamma_R = 1$ meV, $k_B T_L = 10$ meV and $k_B T_R = 15$ meV, $E_0 = [15 + 15 \sin(\Omega t + \phi)]$ meV, $\hbar\Gamma_L = [2 + \sin(\Omega t)]$ meV, and $\Omega = 2\pi/\mathcal{T}_p$.

and the efficiency $\langle \eta \rangle_p$ in driven systems, compared to the steady-state ones. For ϵ_p in Eq. (28), it is always greater than the lower bound $\epsilon_{\text{bound}} \equiv 2/[1 + \langle W_{\text{out}} \rangle_{\text{geo}}/\langle W_{\text{out}} \rangle_{\text{dyn}}]^2$. Hence, once the geometric-phase-induced output work emerges, i.e. $\langle W_{\text{out}} \rangle_{\text{geo}} \neq 0$, the lower limit of ϵ_p is generally unequal to the static counterpart 2, which is also exhibited in Fig. 3(c). Interestingly, as the geometric component exceeds the dynamic one, the lower bound may even approach 0, e.g., $\phi = \pi/8$. Such picture can be alternatively explained that though the output work is strongly enhanced by the geometric effect [Fig. 6(a)], the entropy production is not significantly increased [Fig. 3(d)]. Similarly, $\langle \eta \rangle_{\text{bound}} - \langle \eta \rangle_p \geq 0$ is always satisfied, with the upper bound $\langle \eta \rangle_{\text{bound}}$ given in Eq. (9) and Eq. (12) for $\langle W_I \rangle > 0$ and $\langle W_I \rangle < 0$, respectively. This is also illustrated in Figs. 5(d) and 6(d). In the positive input energy generation regime, as the geometric-phase-induced work dominates the output work, i.e., $\langle W_{\text{out}} \rangle_{\text{geo}} \gg \langle W_{\text{out}} \rangle_{\text{dyn}}$, the entropy production $\langle \sigma \rangle$ is comparatively negligible to $\langle W_{\text{out}} \rangle_{\text{geo}}/T$, which results in the upper bound approaching the unity. While for the case of negative input energy, the efficiency bound can also reach the unity by further considering $\langle W_I \rangle \ll \langle W_{\text{out}} \rangle_{\text{geo}}$. Hence, this shows

the significance of geometric-phase in bounding the efficiency of heat engines by observing the fluctuation of output work. Moreover, such results are in agreement with comparable counterparts in the stochastic clock [41]. Therefore, we conclude that geometric part contribution is incredible to dramatically modify the TUR.

IV. CONCLUSIONS

In summary, for periodically driven systems, we have proposed a class of inequalities, termed as geometric TUR, that relate the entropy production, with the mean of current and its variance by bringing to light the Berry-phase-like effect. This leads to a general trade-off relation between the output work, effective efficiency, entropy production, and an external control protocol. The corresponding bounds indicate that the geometric phase plays a key role in constraining the relative fluctuation of currents. Moreover, such bounds provide insight into the understanding of the precision of thermoelectric heat engine. We note that our theory is able to be applied to systems arbitrarily far from equilibrium, and does not assume any specific symmetry of the system. To demonstrate the practical applicability of our results, we work out the example of a two-terminal single level QD system, which lies within the family of thermoelectric heat engine. Our work paves the way for TUR from the geometric origin and optimizing more complex periodically driven thermoelectric heat engines.

V. ACKNOWLEDGEMENTS

J.L., Z.W., J.P., and J.R. acknowledge the support by the National Natural Science Foundation of China (Grant Nos. 11935010 and 11775159), the Natural Science Foundation of Shanghai (Grant Nos. 18ZR1442800 and 18JC1410900). C.W. acknowledges support from the National Natural Science Foundation of China (Grant No. 11704093) and the Opening Project of Shanghai Key Laboratory of Special Artificial Microstructure Materials and Technology. J.-H.J acknowledges support from the Natural Science Foundation of China (NSFC) (Grant Nos. 12074281, 12047541, and 12074279), the Major Program of Natural Science Research of Jiangsu Higher Education Institutions (Grant No. 18KJA140003), the Jiangsu specially appointed professor funding, and the Academic Program Development of Jiangsu Higher Education (PAPD).

-
- [1] P. Jung, “Periodically driven stochastic systems,” *Phys. Rep.* **234**, 175–295 (1993).
 - [2] M. Esposito, U. Harbola, and S. Mukamel, “Nonequilibrium fluctuations, fluctuation theorems, and counting statistics in quantum systems,” *Rev. Mod. Phys.* **81**, 1665–1702 (2009).
 - [3] M. Campisi, P. Hänggi, and P. Talkner, “Colloquium: Quantum fluctuation relations: Foundations and applications,” *Rev. Mod. Phys.* **83**, 771–791 (2011).
 - [4] U. Seifert, “Stochastic thermodynamics, fluctuation theorems and molecular machines,” *Rep. Prog. Phys.* **75**, 126001 (2012).
 - [5] J. P. Pekola and B. Karimi, “Colloquium: Quantum heat transport in condensed matter systems,” *Rev. Mod. Phys.* **93**, 041001 (2021).
 - [6] J.-H. Jiang and Y. Imry, “Linear and nonlinear mesoscopic thermoelectric transport with coupling with heat baths,” *C. R. Phys.* **17**, 1047 – 1059 (2016).
 - [7] G. Benenti, G. Casati, K. Saito, and R. S. Whitney, “Fundamental aspects of steady-state conversion of heat to work at the nanoscale,” *Phys. Rep.* **694**, 1 (2017).
 - [8] R. Wang, C. Wang, J. Lu, and J.-H. Jiang, “Inelastic thermoelectric transport and fluctuations in mesoscopic system,” [arXiv:2112.09273](https://arxiv.org/abs/2112.09273) (2021).
 - [9] A. C. Barato and U. Seifert, “Thermodynamic uncertainty relation for biomolecular processes,” *Phys. Rev. Lett.* **114**, 158101 (2015).
 - [10] Y. Hasegawa, “Thermodynamic uncertainty relation for general open quantum systems,” *Phys. Rev. Lett.* **126**, 010602 (2021).
 - [11] J. Liu and D. Segal, “Thermodynamic uncertainty relation in quantum thermoelectric junctions,” *Phys. Rev. E* **99**, 062141 (2019).
 - [12] A. M. Timpanaro, G. Guarnieri, J. Goold, and G. T. Landi, “Thermodynamic uncertainty relations from exchange fluctuation theorems,” *Phys. Rev. Lett.* **123**, 090604 (2019).
 - [13] P. Pietzonka and U. Seifert, “Universal trade-off between power, efficiency, and constancy in steady-state heat engines,” *Phys. Rev. Lett.* **120**, 190602 (2018).
 - [14] J. M. Horowitz and T. R. Gingrich, “Thermodynamic uncertainty relations constrain non-equilibrium fluctuations,” *Nat. Phys.* **16**, 15–20 (2020).
 - [15] G. Falasco, M. Esposito, and J.-C. Delvenne, “Unifying thermodynamic uncertainty relations,” *New J. Phys.* **22**, 053046 (2020).
 - [16] A. Dechant and S.-i. Sasa, “Fluctuation–response inequality out of equilibrium,” *Proc. Natl. Acad. Sci. USA* **117**, 6430–6436 (2020).
 - [17] K. Liu, Z. Gong, and M. Ueda, “Thermodynamic uncertainty relation for arbitrary initial states,” *Phys. Rev. Lett.* **125**, 140602 (2020).
 - [18] H. M. Friedman, B. K. Agarwalla, O. Shein-Lumbroso, O. Tal, and D. Segal, “Thermodynamic uncertainty relation in atomic-scale quantum conductors,” *Phys. Rev. B* **101**, 195423 (2020).
 - [19] Y. Hasegawa, “Quantum thermodynamic uncertainty relation for continuous measurement,” *Phys. Rev. Lett.* **125**, 050601 (2020).
 - [20] S. Pal, S. Saryal, D. Segal, T. S. Mahesh, and B. K. Agarwalla, “Experimental study of the thermodynamic uncertainty relation,” *Phys. Rev. Research* **2**, 022044 (2020).
 - [21] D. Hartich and A. Godec, “Thermodynamic uncertainty relation bounds the extent of anomalous diffusion,” *Phys. Rev. Lett.* **127**, 080601 (2021).
 - [22] Y. Hasegawa, “Irreversibility, loschmidt echo, and thermodynamic uncertainty relation,” *Phys. Rev. Lett.* **127**, 240602 (2021).
 - [23] J. Liu and D. Segal, “Coherences and the thermodynamic uncertainty relation: Insights from quantum absorption refrigerators,” *Phys. Rev. E* **103**, 032138 (2021).
 - [24] T. R. Gingrich, J. M. Horowitz, N. Perunov, and J. L. England, “Dissipation bounds all steady-state current fluctuations,” *Phys. Rev. Lett.* **116**, 120601 (2016).
 - [25] P. Pietzonka, F. Ritort, and U. Seifert, “Finite-time generalization of the thermodynamic uncertainty relation,” *Phys. Rev. E* **96**, 012101 (2017).
 - [26] K. Macieszczak, K. Brandner, and J. P. Garrahan, “Unified thermodynamic uncertainty relations in linear response,” *Phys. Rev. Lett.* **121**, 130601 (2018).
 - [27] K. Proesmans and J. M. Horowitz, “Hysteretic thermodynamic uncertainty relation for systems with broken time-reversal symmetry,” *J. Stat. Mech.* **2019**, 054005 (2019).
 - [28] S. Saryal, M. Gerry, I. Khait, D. Segal, and B. K. Agarwalla, “Universal bounds on fluctuations in continuous thermal machines,” *Phys. Rev. Lett.* **127**, 190603 (2021).
 - [29] B. K. Agarwalla and D. Segal, “Assessing the validity of the thermodynamic uncertainty relation in quantum systems,” *Phys. Rev. B* **98**, 155438 (2018).
 - [30] K. Proesmans and C. Van den Broeck, “Discrete-time thermodynamic uncertainty relation,” *Europhys. Lett.* **119**, 20001 (2017).
 - [31] T. Koyuk and U. Seifert, “Operationally accessible bounds on fluctuations and entropy production in periodically driven systems,” *Phys. Rev. Lett.* **122**, 230601 (2019).
 - [32] T. Koyuk and U. Seifert, “Thermodynamic uncertainty relation for time-dependent driving,” *Phys. Rev. Lett.* **125**, 260604 (2020).
 - [33] S. Saryal, S. Mohanta, and B. K. Agarwalla, “Universal bounds on fluctuations for machines with broken time-reversal symmetry,” [arXiv:2110.05297](https://arxiv.org/abs/2110.05297) (2021).
 - [34] K. Brandner, M. Bauer, and U. Seifert, “Universal coherence-induced power losses of quantum heat engines

- in linear response,” *Phys. Rev. Lett.* **119**, 170602 (2017).
- [35] T. Van Vu and Y. Hasegawa, “Thermodynamic uncertainty relations under arbitrary control protocols,” *Phys. Rev. Research* **2**, 013060 (2020).
- [36] K. Brandner, “Coherent transport in periodically driven mesoscopic conductors: From scattering amplitudes to quantum thermodynamics,” *Z. Naturforsch. A* **75**, 483–500 (2020).
- [37] S. Saryal, O. Sadekar, and B. K. Agarwalla, “Thermodynamic uncertainty relation for energy transport in a transient regime: A model study,” *Phys. Rev. E* **103**, 022141 (2021).
- [38] H. J. D. Miller, M. H. Mohammady, M. Perarnau-Llobet, and G. Guarnieri, “Thermodynamic uncertainty relation in slowly driven quantum heat engines,” *Phys. Rev. Lett.* **126**, 210603 (2021).
- [39] E. Potanina, C. Flindt, M. Moskalets, and K. Brandner, “Thermodynamic bounds on coherent transport in periodically driven conductors,” *Phys. Rev. X* **11**, 021013 (2021).
- [40] P. Menczel, E. Loisa, K. Brandner, and C. Flindt, “Thermodynamic uncertainty relations for coherently driven open quantum systems,” *J. Phys. A: Math. Theor.* **54**, 314002 (2021).
- [41] A. C. Barato and U. Seifert, “Cost and precision of brownian clocks,” *Phys. Rev. X* **6**, 041053 (2016).
- [42] T. Koyuk, U. Seifert, and P. Pietzonka, “A generalization of the thermodynamic uncertainty relation to periodically driven systems,” *J. Phys. A: Math. Theor.* **52**, 02LT02 (2018).
- [43] K. Brandner, K. Saito, and U. Seifert, “Thermodynamics of micro- and nano-systems driven by periodic temperature variations,” *Phys. Rev. X* **5**, 031019 (2015).
- [44] K. Brandner and K. Saito, “Thermodynamic geometry of microscopic heat engines,” *Phys. Rev. Lett.* **124**, 040602 (2020).
- [45] Gavin E. Crooks, “Measuring thermodynamic length,” *Phys. Rev. Lett.* **99**, 100602 (2007).
- [46] P. W. Brouwer, “Scattering approach to parametric pumping,” *Phys. Rev. B* **58**, R10135–R10138 (1998).
- [47] N. A. Sinitsyn and I. Nemenman, “Universal geometric theory of mesoscopic stochastic pumps and reversible ratchets,” *Phys. Rev. Lett.* **99**, 220408 (2007).
- [48] N. A. Sinitsyn and I. Nemenman, “The berry phase and the pump flux in stochastic chemical kinetics,” *Europhys Lett.* **77**, 58001 (2007).
- [49] J. Ren, P. Hänggi, and B. Li, “Berry-phase-induced heat pumping and its impact on the fluctuation theorem,” *Phys. Rev. Lett.* **104**, 170601 (2010).
- [50] T. Chen, X.-B. Wang, and J. Ren, “Dynamic control of quantum geometric heat flux in a nonequilibrium spin-boson model,” *Phys. Rev. B* **87**, 144303 (2013).
- [51] H. J. D. Miller and M. Mehboudi, “Geometry of work fluctuations versus efficiency in microscopic thermal machines,” *Phys. Rev. Lett.* **125**, 260602 (2020).
- [52] Z. Wang, L. Wang, J. Chen, C. Wang, and J. Ren, “Geometric heat pump: Controlling thermal transport with time-dependent modulations,” *Front. Phys.* **17**, 1–14 (2022).
- [53] Z. Wang, J. Chen, Z. Liu, and J. Ren, “Observation of geometric heat pump effect in periodic driven thermal diffusion,” *arXiv:2110.10001* (2021).
- [54] G. Manzano, R. Sánchez, R. Silva, G. Haack, J. B. Brask, N. Brunner, and P. P. Potts, “Hybrid thermal machines: Generalized thermodynamic resources for multitasking,” *Phys. Rev. Research* **2**, 043302 (2020).
- [55] T. Yuge, T. Sagawa, A. Sugita, and H. Hayakawa, “Geometrical pumping in quantum transport: Quantum master equation approach,” *Phys. Rev. B* **86**, 235308 (2012).
- [56] C. Wang, J. Ren, and J. Cao, “Unifying quantum heat transfer in a nonequilibrium spin-boson model with full counting statistics,” *Phys. Rev. A* **95**, 023610 (2017).
- [57] Y. Hino and H. Hayakawa, “Geometrical formulation of adiabatic pumping as a heat engine,” *Phys. Rev. Research* **3**, 013187 (2021).
- [58] Y. Izumida, “Hierarchical onsager symmetries in adiabatically driven linear irreversible heat engines,” *Phys. Rev. E* **103**, L050101 (2021).
- [59] J.-H. Jiang, “Thermodynamic bounds and general properties of optimal efficiency and power in linear responses,” *Phys. Rev. E* **90**, 042126 (2014).
- [60] J.-H. Jiang, B. K. Agarwalla, and D. Segal, “Efficiency statistics and bounds for systems with broken time-reversal symmetry,” *Phys. Rev. Lett.* **115**, 040601 (2015).
- [61] V. Holubec and A. Ryabov, “Cycling tames power fluctuations near optimum efficiency,” *Phys. Rev. Lett.* **121**, 120601 (2018).
- [62] Crispin Gardiner and Peter Zoller, *Quantum noise: a handbook of Markovian and non-Markovian quantum stochastic methods with applications to quantum optics* (Springer Science & Business Media, 2004).
- [63] D. Segal, “Heat flow in nonlinear molecular junctions: Master equation analysis,” *Phys. Rev. B* **73**, 205415 (2006).
- [64] B. K. Agarwalla, J.-H. Jiang, and D. Segal, “Full counting statistics of vibrationally assisted electronic conduction: Transport and fluctuations of thermoelectric efficiency,” *Phys. Rev. B* **92**, 245418 (2015).
- [65] B. K. Agarwalla, J.-H. Jiang, and D. Segal, “Quantum efficiency bound for continuous heat engines coupled to noncanonical reservoirs,” *Phys. Rev. B* **96**, 104304 (2017).
- [66] D. Segal, “Stochastic pumping of heat: Approaching the carnot efficiency,” *Phys. Rev. Lett.* **101**, 260601 (2008).
- [67] J.-H. Jiang, O. Entin-Wohlman, and Y. Imry, “Thermoelectric three-terminal hopping transport through one-dimensional nanosystems,” *Phys. Rev. B* **85**, 075412 (2012).
- [68] J.-H. Jiang, M. Kulkarni, D. Segal, and Y. Imry, “Phonon thermoelectric transistors and rectifiers,” *Phys.*

- Rev. B **92**, 045309 (2015).
- [69] J. Lu, R. Wang, C. Wang, and J.-H. Jiang, “Brownian thermal transistors and refrigerators in mesoscopic systems,” *Phys. Rev. B* **102**, 125405 (2020).
 - [70] J. Lu, J.-H. Jiang, and Y. Imry, “Unconventional four-terminal thermoelectric transport due to inelastic transport: Cooling by transverse heat current, transverse thermoelectric effect, and maxwell demon,” *Phys. Rev. B* **103**, 085429 (2021).
 - [71] G. Chen, *Nanoscale Energy Transport and Conversion* (Oxford University Press, London, 2005).
 - [72] H. Haug and A. P. Jauho, *Quantum Kinetics in Transport and Optics of Semiconductors* (Springer-Verlag Berlin Heidelberg, 2008).
 - [73] J. Lu, R. Wang, J. Ren, M. Kulkarni, and J.-H. Jiang, “Quantum-dot circuit-qed thermoelectric diodes and transistors,” *Phys. Rev. B* **99**, 035129 (2019).
 - [74] M. F. Ludovico, L. Arrachea, M. Moskalets, and D. Sánchez, “Probing the energy reactance with adiabatically driven quantum dots,” *Phys. Rev. B* **97**, 041416 (2018).
 - [75] G. Li, B.-Z. Hu, N. Yang, and J.-T. Lü, “Temperature-dependent thermal transport of single molecular junctions from semiclassical langevin molecular dynamics,” *Phys. Rev. B* **104**, 245413 (2021).
 - [76] J. Ren, S. Liu, and B. Li, “Geometric heat flux for classical thermal transport in interacting open systems,” *Phys. Rev. Lett.* **108**, 210603 (2012).
 - [77] M. V. Berry, “Quantal phase factors accompanying adiabatic changes,” *Proc. R. Soc. London A* **392**, 45 (1984).
 - [78] A. Bohm, A. Mostafazadeh, H. Koizumi, Q. Niu, and J. Zwanziger, *The Geometric phase in quantum systems* (Springer-Verlag, New York, 2003).
 - [79] A. Solfanelli, M. Falsetti, and M. Campisi, “Nonadiabatic single-qubit quantum otto engine,” *Phys. Rev. B* **101**, 054513 (2020).
 - [80] L. M. Cangemi, M. Carrega, A. De Candia, V. Cataudella, G. De Filippis, M. Sassetti, and G. Benenti, “Optimal energy conversion through antiadiabatic driving breaking time-reversal symmetry,” *Phys. Rev. Research* **3**, 013237 (2021).
 - [81] N. Piccione, G. De Chiara, and B. Bellomo, “Power maximization of two-stroke quantum thermal machines,” *Phys. Rev. A* **103**, 032211 (2021).
 - [82] B. Bhandari, P. T. Alonso, F. Taddei, F. von Oppen, R. Fazio, and L. Arrachea, “Geometric properties of adiabatic quantum thermal machines,” *Phys. Rev. B* **102**, 155407 (2020).
 - [83] J. Liu, K. A. Jung, and D. Segal, “Periodically driven quantum thermal machines from warming up to limit cycle,” *Phys. Rev. Lett.* **127**, 200602 (2021).
 - [84] P. T. Alonso, P. Abiuso, M. Perarnau-Llobet, and L. Arrachea, “Geometric optimization of non-equilibrium adiabatic thermal machines and implementation in a qubit system,” *arXiv:2109.12648* (2021).
 - [85] G. Jaliel, R. K. Puddy, R. Sánchez, A. N. Jordan, B. Sothmann, I. Farrer, J. P. Griffiths, D. A. Ritchie, and C. G. Smith, “Experimental realization of a quantum dot energy harvester,” *Phys. Rev. Lett.* **123**, 117701 (2019).
 - [86] O. Maillet, P. A. Erdman, V. Cavina, B. Bhandari, E. T. Mannila, J. T. Peltonen, A. Mari, F. Taddei, C. Jarzynski, V. Giovannetti, and J. P. Pekola, “Optimal probabilistic work extraction beyond the free energy difference with a single-electron device,” *Phys. Rev. Lett.* **122**, 150604 (2019).
 - [87] M. Josefsson, A. Svilans, A. M. Burke, E. A. Hoffmann, S. Fahlvik, C. Thelander, M. Leijnse, and H. Linke, “A quantum-dot heat engine operating close to the thermodynamic efficiency limits,” *Nat. Nanotech.* **13**, 920–924 (2018).
 - [88] M. F. Ludovico, L. Arrachea, M. Moskalets, and D. Sanchez, “Periodic energy transport and entropy production in quantum electronics,” *Entropy* **18** (2016), 10.3390/e18110419.
 - [89] J.-H. Jiang, “Enhancing efficiency and power of quantum-dots resonant tunneling thermoelectrics in three-terminal geometry by cooperative effects,” *J. Appl. Phys.* **116**, 194303 (2014).
 - [90] M. F. Ludovico, M. Moskalets, D. Sánchez, and L. Arrachea, “Dynamics of energy transport and entropy production in ac-driven quantum electron systems,” *Phys. Rev. B* **94**, 035436 (2016).
 - [91] M. F. Ludovico, F. Battista, F. von Oppen, and L. Arrachea, “Adiabatic response and quantum thermoelectrics for ac-driven quantum systems,” *Phys. Rev. B* **93**, 075136 (2016).
 - [92] J. Lu, R. Wang, Y. Liu, and J.-H. Jiang, “Thermoelectric cooperative effect in three-terminal elastic transport through a quantum dot,” *J. Appl. Phys.* **122**, 044301 (2017).
 - [93] J.-H. Jiang and Y. Imry, “Enhancing thermoelectric performance using nonlinear transport effects,” *Phys. Rev. Applied* **7**, 064001 (2017).